

**Kinetic energy distribution of OH<sup>+</sup> from water fragmentation by electron impact**

Natalia Ferreira\*

*CEFET-RJ, 20271-110 Rio de Janeiro, Rio de Janeiro, Brazil*

L. Sigaud†

*Universidade Federal Fluminense, 24210-346 Niteroi, Rio de Janeiro, Brazil*

E. C. Montenegro‡

*Universidade Federal do Rio de Janeiro (UFRJ), 21941-972 Rio de Janeiro, Rio de Janeiro, Brazil*

(Received 11 May 2017; published 18 July 2017)

The release of the highly reactive radical OH<sup>+</sup> from the fragmentation of water by electron impact is made mostly through the OH<sup>+</sup> + H<sup>0</sup> channel. This channel ejects suprathreshold OH<sup>+</sup> ions with a kinetic energy distribution whose details are unexplored so far due to the difficulty in experimentally characterizing ions ejected with very low kinetic energy without another charged partner. These ions are studied here using the delayed extraction time-of-flight technique (DETOF). The structures and substructures in the kinetic energy distribution of OH<sup>+</sup> associated with both single and double ionization are identified qualitatively and quantitatively. A comparison with the kinetic energy distribution of the complementary channel OH<sup>0</sup> + H<sup>+</sup>, also originating from vacancies in the 1b<sub>2</sub> orbital, shows marked differences between the two, mainly regarding the relative role between the fragmentation involving the H<sub>2</sub>O<sup>+</sup> ground state or via transitions to repulsive states.

DOI: [10.1103/PhysRevA.96.012705](https://doi.org/10.1103/PhysRevA.96.012705)**I. INTRODUCTION**

Of all the ions originated from water fragmentation by electron or swift proton impact, the most abundant among them is OH<sup>+</sup> [1,2]. It turns out that OH<sup>+</sup> is an extremely powerful radical and plays a key role in postcollision chemistry of any water-based environment subjected to radiation. The striking influence of this ionic radical can be seen in a wide variety of situations, such as in the establishment of the molecular inventory of cometary [3] and planetary magnetospheres [4], in the inventory of atmospheres of icy moons [5–7], in the amount and types of water radiolysis products [8,9], in biological effects of radiation [10,11], and in radiation therapy [12].

The electronic configuration of the ground state of water is (1a<sub>1</sub>)<sup>2</sup> (2a<sub>1</sub>)<sup>2</sup> (1b<sub>2</sub>)<sup>2</sup> (3a<sub>1</sub>)<sup>2</sup> (1b<sub>1</sub>)<sup>2</sup>. Under the impact of ionizing radiation, be it photons, electrons, or heavy ions, the water molecule can fragment into two or three bodies, depending on the energy transferred in the collision and in which molecular orbital a primary vacancy is produced. Tan *et al.* [13], in their study on photofragmentation of water, accomplished relating the fragmentation pathways to the primary vacancies created, assigning vacancies in the 1b<sub>2</sub> orbital as the ones responsible for OH<sup>+</sup> + H<sup>0</sup> production. Later, water fragmentation measurements by electrons [14,15], protons [16], and heavy ions [17] provided a clear signature that OH<sup>+</sup> could also be produced by the Auger decay of vacancies created in the 2a<sub>1</sub> orbital, in this case giving OH<sup>+</sup> + H<sup>+</sup> as fragmentation products. The branching ratios associated with the fragmentation pathways for vacancies created in each of the molecular orbitals established by Tan *et al.* [13]

were later complemented by the branching ratios associated with the Auger decay [14,15].

These branching ratios and pathways of fragmentation were determined empirically. The mechanisms responsible for the redistribution of energy from the production of primary vacancies had not been unveiled until recently. In an effort to fill this conceptual gap, Suárez *et al.* [18] were able to calculate the branching ratios associated with the fragmentation channels OH<sup>+</sup> + H<sup>0</sup> and OH<sup>0</sup> + H<sup>+</sup> from vacancies in the 1b<sub>2</sub> orbital. These calculations show that although fragmentation results in two moieties, the three bodies actively participate in the vibronic coupling that leads to fragmentation. The experimental branching ratios can be reproduced by considering that the relaxation of the 1b<sub>2</sub> orbital involves a rapid orbital transfer via a conical intersection accompanied by a Renner-Teller coupling in a linear configuration of the molecule.

In such a conceptual context other important features associated with fragmentation are difficult to unravel. One of them is the kinetic energy distribution (KED) of the fragments, usually visualized by the shape of the potential energy curves with respect to the separation distance of the two moieties from the Frank-Condon region. This procedure is difficult to perform if several potential curves that change shape with the changing bending angle are involved in fragmentation. Furthermore, a point of great conceptual and practical interest with respect to the two fragmentation channels, originating from vacancies in the 1b<sub>2</sub> orbital, is related to possible differences in their kinetic energy release distribution (KERD). These differences were suggested earlier by Powis and Reynolds [19] and are shown here to be striking, a conclusion obtained by comparing the present KERD for the OH<sup>+</sup> + H<sup>0</sup> channel with the KERD for the OH<sup>0</sup> + H<sup>+</sup> pathway, obtained from the H<sup>+</sup> distributions previously measured by de Barros *et al.* [20] for electron impact.

\*nataferr@gmail.com

†lsigaud@if.uff.br

‡montenegro@if.uff.br

From the experimental perspective, the identification of details in the KED structures that might lead to a better understanding of the fragmentation mechanisms is also limited. The main reason is because there are not many available techniques to select the kinetic energy of slow, suprathermal ionic fragments which are not accompanied by a second ion that can be used for an extra selection of events. The  $\text{OH}^+ + \text{H}^0$  channel fits into this scenario. For fragmentation channels involving larger kinetic energy release, such as  $\text{OH}^+ + \text{H}^+$ , some measurements of the KERD have been reported for both cases of heavy-ion impact, mostly at low projectile velocities [21–24], and of electron impact [25,26].

In addition to the limited conceptual and empirical understandings mentioned above, this scenario counteracts the needs of many applications in which the KED of the fragments is required in a greater level of detail. Indeed, in many environments, the kinetic energy distribution of the OH, O, and H products of the water fragmentation, charged or not, is an important component behind its evolution from the primary ionizing event. Examples in water-based environments submitted to radiation are the relationship between the KED and the escape velocity of icy moons in the establishment of their atmospheric inventories, or in subsequent charge transfer reactions, like  $\text{OH}^+ + \text{H}_2\text{O} \rightarrow \text{H}_2\text{O}^+ + \text{OH}$ , usually highly sensitive to the relative velocity between the participants.

In this work the signatures of the  $\text{OH}^+ + \text{H}^0$  and  $\text{OH}^+ + \text{H}^+$  channels in the KED of the  $\text{OH}^+$  fragment produced by electron impact are identified and clearly separated. The sensitivity of the delayed extraction time-of-flight (DETOF) technique to characterize the kinetic energy distribution of slow fragments is here advantageously used to this end.

## II. EXPERIMENT

The energy distribution of the  $\text{OH}^+$  fragment was measured using the already established DETOF methodology [27–29]. This technique consists of intentionally and gradually retarding the extraction of the collisional products in a time-of-flight (TOF) mass spectrometer so that it becomes possible to progressively exclude, from the TOF collection region, fragment ions with higher velocities. The apparatus itself consists of an electron gun coupled with a gas cell, and its interaction region is connected to a double-focusing TOF spectrometer, which is described in detail elsewhere [30]. The electron energy ranges from 30 to 700 eV, with the gun emitting pulses 50 ns long with a repetition rate of 20 kHz, while the gas cell is kept at a  $10^{-4}$  Torr pressure environment. This setup guarantees a single-collisional regime, and the ions formed are extracted by a  $21 \text{ kV m}^{-1}$  electrostatic square pulse, which guides the ions through the TOF tube. Finally, the produced ions are collected in a MCP (microchannel plate) detector and the produced signal is analyzed by standard time-resolved electronics. The electron current is measured by a Faraday cup, and the cell pressure is monitored by an absolute manometer, allowing the measurements to be normalized and, thus, making it possible to obtain absolute cross sections for each positively charged fragment. For each electron energy, a set of around 50 measurements is taken varying the time delay between the electron beam pulse and the extraction field, and afterwards is normalized by the number of incident electrons and scattering

centers. Then, this set is analyzed converting from the time delay space to the velocity (energy) space. The number of collected products of the species of interest at a time delay  $t$ ,  $\text{OH}^+(t)$ , is compared to the number of the same fragment at the minimum delay time of  $t_0 = 300 \text{ ns}$  [30],  $\text{OH}^+(t = t_0)$ , therefore evaluating the fraction of ions present after a certain time delay.  $\text{OH}^+(t)$  can be expressed as

$$\text{OH}^+(t) = \int_0^\infty n_T(v_\perp, t) f(v_\perp) dv_\perp, \quad (1)$$

where  $n_T(v_\perp, t)$  is a known function that takes into account both the free flight time of the ions before the extraction field is turned on and the geometry of the spectrometer [27–29], which can be calculated analytically, and  $f(v_\perp)$  corresponds to the velocity distribution of the ion. Since the unknown velocity distribution is part of the integrand, Eq. (1) is a Fredholm-type equation and cannot be solved analytically. Therefore, trial energy distribution functions  $f(E)$  are used, which are afterwards converted to correspondent velocity distributions to solve Eq. (1) numerically and then compared to the amount of fragments measured over the range of time delays. There are three kinds of normalized energy distributions used in this manner, representing different processes for that particular species with a specific mass-to-charge ratio in a TOF spectrum: (i) Maxwell-Boltzmann (MB), which has no free parameters and accounts for moieties that acquire no kinetic energy in the ionization process, namely the unfragmented parent ion with any charge state; (ii) Exponential (Expo), representing slow products with suprathermal kinetic energy, coming from fragmentation via vibrational continuum [31]; and (iii) Gaussian (G), corresponding to more energetic fragments, formed in more violent collisions leading to dissociative states of the molecule. The parameters of the exponential and Gaussian distributions, such as their average energy and their standard deviation, are related to the inflexions present on the measured  $\text{OH}^+(t)/\text{OH}^+(t = t_0)$  ratio against the time delay, as can be seen in Fig. 1. The kinetic energy distributions are then optimized to best adjust their sum to the experimental data. The uncertainties are estimated by varying the distributions parameters around the optimum configuration, maintaining a criterion that the coefficient of determination,  $R$ -squared ( $R^2$ ) [32],

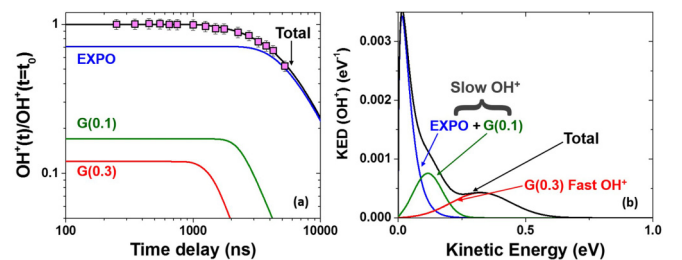


FIG. 1. (a) Ratios (squares) between the  $\text{OH}^+$  yield for different time delays  $t$  and the  $\text{OH}^+$  yield for the minimum time delay  $t_0$  of 300 ns for 450-eV impact energy. The fit to the data (black lines) is given by the sum of the following distributions: one exponential, Expo (blue lines); one Gaussian centered at 0.1 eV, G(0.1) (green lines); and one Gaussian centered at 0.3 eV, G(0.3) (red lines). (b) Corresponding energy distributions as a function of the  $\text{OH}^+$  kinetic energy.

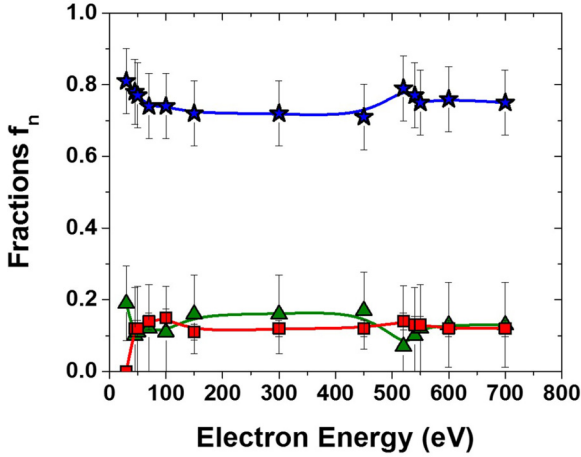


FIG. 2. Dependence, with the projectile energy, of the relative yields of the normalized OH<sup>+</sup> kinetic energy distribution:  $f_1$  (stars),  $f_2$  (triangles), and  $f_3$  (squares). The lines are to guide the eye.

is kept above 0.97. The total energy distribution, being the properly weighted sum of the energy distributions used to fit the experimental data, for the OH<sup>+</sup> fragment can be written as

$$f(E) = f_1[\alpha_1 e^{-\alpha_1 E}] + f_2 \left[ \frac{2\alpha_2}{\sqrt{\pi}[1 + \operatorname{erf}(\alpha_2 E_2)]} e^{-\alpha_2^2(E-E_2)^2} \right] + f_3 \left[ \frac{2\alpha_3}{\sqrt{\pi}[1 + \operatorname{erf}(\alpha_3 E_3)]} e^{-\alpha_3^2(E-E_3)^2} \right]. \quad (2)$$

where  $f_1$ ,  $f_2$ , and  $f_3$  are the relative weights of the normalized energy distributions. The parameters  $\alpha_n$  and  $E_n$  are the adjustable parameters for each energy distribution. It should be noted that, while the parameters of the energy distributions themselves remain constant for all measurements, the  $f_n$  values depend on the electron impact energy. For example, the relative weights for 450 eV, shown in Fig. 1, are  $\{f_1, f_2, f_3\} = \{0.71, 0.17, 0.12\}$ ,  $\{\alpha_1, \alpha_2, \alpha_3\} = \{34.56, 11.96, 5.86\} \text{ eV}^{-1}$ ,  $E_2 = 0.1 \text{ eV}$ , and  $E_3 = 0.3 \text{ eV}$ .

The dependence of the relative weights,  $f_n$ , with the projectile energy is shown in Fig. 2. The analysis hints at a small change in the yields near the O 1s ionization energy (543 eV), although the present uncertainties do not allow any quantitative inferences.

### III. RESULTS AND DISCUSSION

The first of our results to be highlighted is the clear separation of the KED of the OH<sup>+</sup> fragments, KED(OH<sup>+</sup>), into two subgroups: one at high energy, associated with the Gaussian centered at 0.3 eV, and a second one at low energy, structured and composed predominantly by the exponential and complemented by a small Gaussian centered at 0.1 eV. The cross sections associated with these structures are indicated as  $\sigma_{G(0.3)}$ ,  $\sigma_{\text{expo}}$ , and  $\sigma_{G(0.1)}$ , respectively. It is naturally tempting to associate these two subgroups with the double-ionization channel, OH<sup>+</sup> + H<sup>+</sup>, and with the single-ionization channel, OH<sup>+</sup> + H<sup>0</sup>, respectively, in a similar way as described in Ref. [33] for the O<sup>+</sup> case. This association is, in fact, fairly direct, as can be seen with the aid of Fig. 3. In

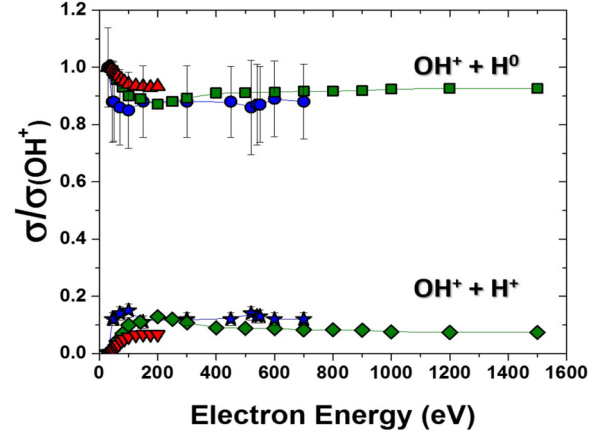


FIG. 3. Ratios of the main structures found in the kinetic energy distribution associated with the OH<sup>+</sup> recoil ion compared to the yields for the single- and double-ionization contributions to the OH<sup>+</sup> fragment as a function of the electron impact energy. OH<sup>+</sup> + H<sup>0</sup> channel:  $(\sigma_{\text{expo}} + \sigma_{G(0.1)})/\sigma_{\text{OH}^+}$  (circles, this work), single ionization coincidence measurements by Montenegro *et al.* [2] (squares) and King and Price [25] (triangles). OH<sup>+</sup> + H<sup>+</sup> channel:  $\sigma_{G(0.3)}/\sigma_{\text{OH}^+}$  (stars, this work), double-ionization coincidence measurements by Montenegro *et al.* [2] (lozenges) and King and Price [25] (inverted triangles). The lines are to guide the eye.

this figure the ratios of the cross sections  $\sigma_{\text{OH}^+ + \text{H}^0}/\sigma_{\text{OH}^+ \text{ total}}$  and  $\sigma_{\text{OH}^+ + \text{H}^+}/\sigma_{\text{OH}^+ \text{ total}}$  taken from Refs. [2] and [25] are displayed together with the ratios  $(\sigma_{G(\text{expo})} + \sigma_{G(0.1)})/\sigma_{\text{OH}^+ \text{ total}}$  and  $\sigma_{G(0.3)}/\sigma_{\text{OH}^+ \text{ total}}$ , from this work. The correlation is clear both in absolute values and in the dependence with the incident electron energy.

#### A. Double-ionization OH<sup>+</sup> + H<sup>+</sup> channel

The energetics of the double-ionization channel OH<sup>+</sup> + H<sup>+</sup> has been studied previously by the impact of electron, photon, and heavy particles and is analyzed first. From the above-identified correlations and using momentum conservation, it is straightforward to see that the Gaussian centered at 0.3 eV corresponds to an average kinetic energy release ( $Q$ ) of 5.4 eV, with a standard deviation of 2.16 eV for all impact energies above 45 eV. King and Price [25] studied this channel by electron impact with energies up to 200 eV and reported a double-peak structure at  $Q = 3.6$  and 9.2 eV, suggesting an average  $Q$  of  $\sim 6.4$  eV. Singh *et al.* [26] found values of  $Q$  ranging from  $\sim 2.5$  to  $\sim 7.0$  eV with an average of 4.3 eV, for a 10-keV electron impact. Richardson *et al.* [34] reported an average  $Q$  of 4.7 eV using HeII (40.8 eV) UV light, while Winkoun *et al.* [35] reported two structures at  $Q = 3.0$  and 5.5 eV for 41-eV photons. A slightly larger average  $Q$  of  $\sim 6$  eV is found if high-energy photons are used to produce an O 1s vacancy [36]. In the case of heavy projectiles, Martin *et al.* [37] used a 3-keV proton impact and found  $Q \sim 5.0$  eV for the average kinetic energy release. These results are reasonably dispersed and may indicate the presence of fine structures that would be more or less emphasized by the specificities of each one of these experiments. Our methodology does not allow the identification of finer structures. However, the excellent agreement obtained for the corresponding branching ratio,

as shown in Fig. 3, allows us to conclude that all eventual contributing structures to the  $\text{OH}^+ + \text{H}^+$  channel are, on average, included in the Gaussian centered at 0.3 eV.

For impact energies up to  $\sim 400$  eV, the double ionization is dominated by direct double impact, where the projectile interacts twice with the target electrons [14–16]. This double-ionization mechanism involves the production of vacancies in various combinations of the outermost valence orbitals [38]. On the other hand, above 400 eV, and increasingly effective at high energies, the  $\text{OH}^+ + \text{H}^+$  production is dominated by the Auger decay of single vacancies produced in the  $2a_1$  orbital [14–16]. Our results show that this change in the prominence of the mechanisms behind double ionization is not remarkably reflected in the  $\text{KED}(\text{OH}^+)$ , which can be, on average, described by the same G(0.3) distribution. It is possible, however, that these two mechanisms are characterized by finer structures that our present resolution is unable to identify.

### B. Single-ionization $\text{OH}^+ + \text{H}^0$ channel

The identification and characterization of the single-ionization channel  $\text{OH}^+ + \text{H}^0$  in the  $\text{KED}(\text{OH}^+)$  are much more scarce. The average  $\text{OH}^+$  kinetic energy corresponding to the joint Expo + G(0.1) distributions is 0.039 eV, which is near the value of 0.034 eV earlier found by Stanton and Monahan [39] for the first moment of the  $\text{KED}(\text{OH}^+)$ . As the Expo distribution has an associated mean kinetic energy of 0.029 eV, slightly above thermal energy, a further analysis of this distribution requires its deconvolution with the Maxwell-Boltzmann distribution to determine its main characteristics in the center of mass (c.m.) of the parent molecule. This can be achieved using the result of Ref. [40] for two-body decay, relating the fragment energy in the c.m. system with the corresponding distribution in the laboratory as a consequence of the thermal motion of the parent molecule. Assuming that the distribution in the c.m. can be also approximated by an exponential,  $\text{Expo}_{\text{c.m.}} = \alpha_{\text{c.m.}} e^{-\alpha_{\text{c.m.}} E}$ , numerical evaluation of the convolution integral gives that  $\alpha_{\text{c.m.}}$  can be related to  $\alpha_1$  by  $\alpha_{\text{c.m.}} = 0.315 \alpha_1^{0.932} (1 - e^{-0.0075(40.83 - \alpha_1)})$  for  $\alpha_1 \leq 37 \text{ eV}^{-1}$ . Thus, using the value of  $\alpha_1$  given previously, one has  $\alpha_{\text{c.m.}} = 186.3$ , resulting in an associated mean  $\text{OH}^+$  kinetic energy of 0.0054 eV in the c.m. system. This corresponds to  $Q = 0.097$  eV which is in good agreement with the value reported by Powis and Reynolds [19] for the  $\text{OD}^+$  kinetic energy release near its appearance energy.

For a two-body system this small value of  $Q$  often indicates that fragmentation occurs via an excitation to some vibrational continuum. In the case of water fragmentation, however, this association is not so obvious since all three bodies actively participate in the process of energy redistribution that results in the fragmentation in two moieties [18]. This redistribution involves the ground state,  $\tilde{X}$ , and the two first excited states,  $\tilde{A}$  and  $\tilde{B}$ , of  $\text{H}_2\text{O}^+$ , which are associated with vacancies in the  $1b_1$ ,  $3a_1$ , and  $1b_2$  orbitals, respectively [41]. These states have very different equilibrium geometries, with angles H-O-H at  $110^\circ$ ,  $180^\circ$ , and  $54^\circ$ , respectively [42], causing strong bending oscillations when transitions between them occur. According to Suárez *et al.* [18], the state  $\tilde{B}$ , corresponding to the original  $1b_2$  vacancy, is rapidly ( $\sim 30$  fs) depopulated to state  $\tilde{A}$  by

means of a conical intersection, reaching the latter out of the equilibrium geometry. A Renner-Teller coupling between states  $\tilde{A}$  and  $\tilde{X}$ , accomplished when this bending motion leads the molecule to a linear geometry ( $180^\circ$ ), feeds progressively the state  $\tilde{X}$  into near the vibrational continuum, leading to  $\text{OH}^+ + \text{H}^0$  fragmentation. This occurs in competition with the fragmentation of state  $\tilde{A}$  which correlates with the  $\text{OH}^0 + \text{H}^+$  channel. These fragmentation routes are expected to give low- $Q$  values and might be the mechanism behind the Expo distribution here identified in the  $\text{OH}^+ + \text{H}^0$  fragmentation. For simplicity, and to give a pictorial analogy to the reader, we are labeling this rather complex process as excitation to the “vibrational continuum.”

The G(0.1) distribution composes the low-energy set associated with the  $\text{OH}^+ + \text{H}^0$  fragmentation and is present in a smaller proportion compared to the Expo one. Its deconvolution to the center of mass makes this distribution narrower but does not significantly change the mean kinetic energy of 0.1 eV of the  $\text{OH}^+$  fragment, which corresponds to  $Q = 1.8$  eV. This value of  $Q$  suggests that G(0.1) may be related to an alternative mechanism for the  $\text{OH}^+ + \text{H}^0$  fragmentation [18,19,43,44] and involve spin-orbit transitions to the repulsive  $\text{H}_2\text{O}^+(\tilde{a}^4B_1)$  state. In this case, and according to the reported energy diagram in Ref. [18], the  $Q$  value would be  $\sim 1.4$  eV, obtained from the energy difference between the lowest crossing point of the  $\tilde{B}^2B_2$  and  $\tilde{a}^4B_1$  potential energy curves and the asymptotic dissociation energy correlated to the  $\text{OH}^+(\tilde{3}\Pi) + \text{H}^0(\tilde{2}S)$  fragments. A slightly smaller value of  $Q \sim 1.3$  eV is obtained if the potential energy curves reported in Ref. [41] are used. It is important to note that these values are just estimates. If we stick to the two-dimensional representation of the evolution of the system through the potential curves, as the system evolves, these curves move up and down accompanying the bending motion of the molecule and changing the energy value at the crossing. Thus,  $Q$ -value estimates obtained from potential energy curves frozen at a particular angle should be considered with caution. A time-dependent evolution is needed to obtain the final KERD of the fragments. Additionally, since the value of  $Q = 1.8$  eV is significantly higher than the value  $Q = 0.0974$  eV associated with the Expo distribution, the former suggests the participation of a repulsive potential in the ejection of the ions associated with G(0.1). As  $\tilde{a}^4B_1$  is the first repulsive potential converging asymptotically to the  $\text{OH}^+ + \text{H}^0$  channel, we tentatively assign the G(0.1) distribution to this last fragmentation pathway. As an additional comment, it should be mentioned that estimates for contributions to the  $Q$  values from other modes of redistribution of energy, such as rotational states, are very uncertain in such a complex environment.

### C. Comparison of KERD of $\text{OH}^+ + \text{H}^0$ and $\text{OH}^0 + \text{H}^+$ channels

A still open question, which would allow a more comprehensive test of the details of the fragmentation pathways associated with the vacancies in the  $1b_2$  orbital, refers to possible differences in the KERD associated with the  $\text{OH}^+ + \text{H}^0$  and  $\text{OH}^0 + \text{H}^+$  channels. The possibility that there are differences in these two KERDs was raised some time ago by Powis and Reynolds [19] and is investigated in this section.

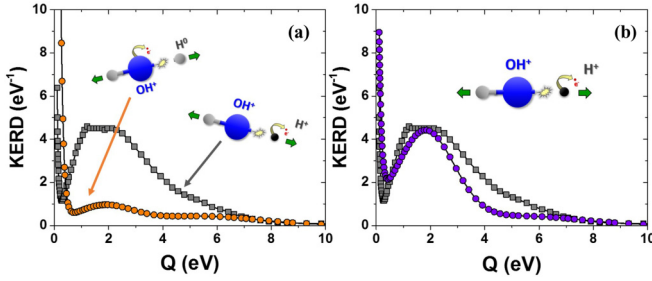


FIG. 4. (a) Comparison between the kinetic energy release distributions for the OH<sup>+</sup> + H<sup>0</sup> channel (this work, circles) and the OH<sup>0</sup> + H<sup>+</sup> channel (from Ref. [20], squares). (b) Same as panel (a) but with the Expo<sub>Q</sub> and G<sub>Q</sub>(1.8) contributions to the OH<sup>+</sup> + H<sup>0</sup> channel adjusted to the OH<sup>0</sup> + H<sup>+</sup> distribution from Ref. [20].

A comparison between the ejection kinematics of these two fragmentation channels can be made through the distribution of the kinetic energy release, KERD. The low-energy portion of these distributions can be obtained from the KED(OH<sup>+</sup>) and KED(H<sup>+</sup>) measured in this work and by de Barros *et al.* [20], respectively, using two-body fragmentation scaling:  $Q = 18E_{\text{OH}^+}$  and  $Q = (18/17)E_{\text{H}^+}$ , where  $E_{\text{OH}^+}$  and  $E_{\text{H}^+}$  are the kinetic energies of the products. In the measurements of Ref. [20], three-body fragmentation, such as H<sup>+</sup> + O<sup>+</sup> + H<sup>0</sup>, is included in the H<sup>+</sup> KED and cannot be scaled by the two-body scaling procedure. However, since the average value of  $Q$  associated with this channel is  $\sim 12$  eV [26], and the cross sections for three-body decay releasing at least one H<sup>+</sup> are significantly smaller than the two-body ones OH<sup>0</sup> + H<sup>+</sup>, it does not influence the shape of the low-energy part of the KERD in which we are interested. Note also that, because the lowest H<sup>+</sup> kinetic energy measured in Ref. [20] is much larger than the thermal energy, no deconvolution with the Maxwell-Boltzmann distribution is needed.

Figure 4(a) displays the normalized KERD obtained from the values reported by de Barros *et al.* [20], which should reproduce the OH<sup>0</sup> + H<sup>+</sup> KERD for  $Q$  smaller than  $\sim 10$  eV, along with the OH<sup>+</sup> + H<sup>0</sup> KERD from our measurements. It is evident from this figure that these two channels of fragmentation do not have the same KERD. In fact, the Expo<sub>Q</sub> and G<sub>Q</sub>(1.8) structures seem to have their weights reversed. The subscript  $Q$  means the OH<sup>+</sup> and H<sup>+</sup> distributions are rescaled to the  $Q$  values.

A quantitative characterization of these differences can be made by adjusting the OH<sup>0</sup> + H<sup>+</sup> KERD by the same three distributions as that of OH<sup>+</sup> + H<sup>0</sup> but normalized to 0.87, instead of 1, to account for the O<sup>+</sup> + H<sup>+</sup> + H<sup>0</sup> channel [26]. This last fragmentation channel has approximately the same weight ( $\sim 0.13$ ) of G<sub>Q</sub>(5.4) associated with the OH<sup>+</sup> + H<sup>+</sup> channel [15,26]. Thus, the weights for the low-energy Expo<sub>Q</sub> and G<sub>Q</sub>(1.8) structures are constrained to  $f_1 + f_2 = 0.74$ . The fractions  $f_1 = 0.13$  and  $f_2 = 0.61$ —in contrast with  $f_1 = 0.75$  and  $f_2 = 0.12$  obtained for the OH<sup>+</sup> + H<sup>0</sup> channel—give the good agreement shown in Fig. 4(b). It is important to emphasize that this good agreement is achieved by assuming that the two KERDs are composed of the same structures [Expo<sub>Q</sub>, G<sub>Q</sub>(1.8), and G<sub>Q</sub>(5.4)], only by varying the relative weights between the first two.

Thus, from the above discussion, it can be seen that the Expo<sub>Q</sub> structure, associated with a fragmentation via an excitation to some vibrational continuum, contributes to  $\sim 75\%$  to the KERD of the OH<sup>+</sup> + H<sup>0</sup>, but only to  $\sim 13\%$  of the OH<sup>0</sup> + H<sup>+</sup> KERD. On the other hand, the G<sub>Q</sub>(1.8) structure contributes to  $\sim 13\%$  of the KERD of the OH<sup>+</sup> + H<sup>0</sup>, but to a larger amount of  $\sim 61\%$  to the OH<sup>0</sup> + H<sup>+</sup> KERD.

Although these two fragmentation channels show very similar structures for the KERD, at least within the present experimental resolution, their associations with the potential energy curves of H<sub>2</sub>O<sup>+</sup> are not straightforward. In particular, the G<sub>Q</sub>(1.8) structure, observed for both OH<sup>+</sup> + H<sup>0</sup> and OH<sup>0</sup> + H<sup>+</sup> channels, cannot be associated with the same repulsive potential energy curve. In fact, the repulsive  $\tilde{a}^4B_1$  state is correlated asymptotically just to the OH<sup>+</sup> + H<sup>0</sup> channel. According to Sage *et al.* [41], the next repulsive potential following  $\tilde{a}^4B_1$  is of the  $^2B_1$  kind, which, in this case, is asymptotically correlated to the OH<sup>0</sup> + H<sup>+</sup> dissociation channel. It turns out that this repulsive  $^2B_1$  state has, by coincidence, the same  $Q \sim 1.3$  as the  $\tilde{a}^4B_1$  taken from the difference between the lowest crossing with  $\tilde{B}^2B_1$  and the asymptotic energy. This numerical result is consistent with the observed similitude of the KERD for these two fragmentation channels and gives support to the tentative assignment of G<sub>Q</sub>(1.8) to each one of these two repulsive potentials correlating to each fragmentation channel. Further calculations focusing at the KERD are needed to elucidate the quantitative results of the measurements.

It might be useful for some applications to have the values of the cross sections of the KED structures of the OH<sup>+</sup>, OH<sup>0</sup>, H<sup>+</sup>, and H<sup>0</sup> fragments, directly related to the ionization cross section of the  $1b_2$  orbital ( $\sigma_{1b_2}$ ). This can be done by combining the current results with the known fragmentation fractions associated with hole creation in given water molecular orbitals [13,15]. The respective fractions for the fragmentation partners are shown in Table I. For example, the cross section for production of H<sup>+</sup> ions with an average kinetic energy of 0.092 eV is equal to  $0.039 \sigma_{1b_2}$ . From this table it can be also concluded that 60.3% of the vacancies produced in the  $1b_2$  orbital result in suprathermal OH<sup>+</sup> ions with an average kinetic energy of 0.0054 eV in the c.m..

#### D. Conclusions

The DETOF technique was used to find the main structures that make up the kinetic energy distribution of the OH<sup>+</sup> radical produced by the ionization of the  $1b_2$  orbital by electron impact. Two contributions were identified which allow the separation of the double ionization from the single ionization. The contribution to the single ionization is structured,

TABLE I. Fractions of vacancies in the  $1b_2$  orbital appearing as subgroups of the KED for the OH<sup>+</sup> + H<sup>0</sup> and OH<sup>0</sup> + H<sup>+</sup> channels. The average  $Q$  for the Expo and G(0.1) distributions are 0.0974 and 1.8 eV, respectively.

Channel	Expo fraction	G(0.1) fraction
OH <sup>+</sup> + H <sup>0</sup>	0.603	0.097
OH <sup>0</sup> + H <sup>+</sup>	0.039	0.181

containing two substructures. The first substructure, with suprathermal kinetic energy in the CM and with an exponential shape, was associated with the  $\text{OH}^+ + \text{H}^0$  fragmentation via the  $\tilde{X}$  vibrational continuum. The second substructure, also associated with the  $\text{OH}^+ + \text{H}^0$  fragmentation, was represented by a Gaussian centered at 0.1 eV and tentatively assigned to a spin-orbit transition to a  $\tilde{a}^4B_1$  repulsive potential. The second contribution, represented by a Gaussian centered at 0.3 eV, was clearly associated with the double-ionization channel  $\text{OH}^+ + \text{H}^+$ . The identification of the substructures in the KERD for the  $\text{OH}^+ + \text{H}^0$  channel, which involves the ejection of only one ion to be detected, had not been previously measured. In addition, through a rescaling of the results of de Barros *et al.* [20], it was possible to verify a marked difference between the relative contributions for the two-body breakup via vibrational continuum and via transitions involving repulsive potentials in the ejection of the  $\text{OH}^+$  and  $\text{OH}^0$  fragments. Most of  $\text{OH}^+$  fragments were ejected with a suprathermal kinetic energy of  $\sim 0.005$  eV,

while the majority of  $\text{OH}^0$  fragments were ejected with a larger kinetic energy,  $\sim 0.1$  eV. These findings should give a more stringent test of theoretical calculations regarding the fragmentation pathways originating from vacancies in the  $1b_2$  orbital. Finally, we should mention that a quite small fraction of the single ionized  $\text{OH}^+ + \text{H}^0$  and  $\text{OH}^0 + \text{H}^+$  channels coming from satellite states near the  $2a_1$  orbital [33] cannot be discarded. However, the identification of their signatures are beyond the detection limits of the present experiment.

#### ACKNOWLEDGMENTS

The authors would like to acknowledge the Brazilian funding agencies Conselho Nacional de Desenvolvimento Científico e Tecnológico (CNPq), Coordenação de Aperfeiçoamento de Pessoal de Nível Superior (CAPES), and Fundação de Amparo à Pesquisa do Rio de Janeiro (FAPERJ). The authors thank to Ismanuel Rabadan for his insightful discussions on fragmentation mechanisms.

- 
- [1] Y. Itikawa and N. Mason, *J. Phys. Chem. Ref. Data* **34**, 1 (2005).  
 [2] E. C. Montenegro, S. W. J. Scully, J. A. Wyer, V. Senthil, and M. B. Shah, *J. Electron Spectrosc. Relat. Phenom.* **155**, 81 (2007).  
 [3] M. Rubin, K. C. Hansen, T. I. Gombosi, M. R. Combi, K. Altwegg, and H. Belsiger, *Icarus* **199**, 505 (2009).  
 [4] M. Blanc, D. J. Andrews, A. J. Coates, D. C. Hamilton, C. M. Jackman, X. Jia, A. Kotova, M. Morooka, H. T. Smith, and J. H. Westlake, *Space Sci. Rev.* **192**, 237 (2015).  
 [5] M. H. Burger, E. C. Sittler, Jr., R. E. Johnson, H. T. Smith, O. J. Tucker, and V. I. Shematovich, *J. Geophys. Res.* **112**, A06219 (2007).  
 [6] V. I. Shematovich, *Solar Syst. Res.* **42**, 473 (2008).  
 [7] T. E. Cravens, R. L. McNutt, Jr., J. H. Waite, Jr., I. P. Robertson, J. G. Luhmann, W. Kasprzak, and W.-H. Ip, *Geophys. Res. Lett.* **36**, L08106 (2009).  
 [8] B. Gervais, M. Beuve, G. H. Olivera, and M. E. Galassi, *Radiat. Phys. Chem.* **75**, 493 (2006).  
 [9] K. G. Reeves and Y. Kanai, *Sci. Rep.* **7**, 40379 (2017).  
 [10] K. Takeshita, K. Fujii, K. Anzai, and T. Ozawa, *Free Radical Biol. Med.* **36**, 1134 (2004).  
 [11] R. M. Abolfath, D. J. Carlson, Z. J. Chen, and R. Nath, *Phys. Med. Biol.* **58**, 7143 (2013).  
 [12] M. Yoshimura, S. Itasaka, H. Harada, and M. Hiraoka, *BioMed Res. Int.* **2013**, 685308 (2013).  
 [13] K. H. Tan, C. E. Brion, Ph. E. Van der Leeuw, and M. J. van der Wiel, *Chem. Phys.* **29**, 299 (1978).  
 [14] S. W. J. Scully, J. A. Wyer, V. Senthil, M. B. Shah, and E. C. Montenegro, *Phys. Rev. A* **73**, 040701(R) (2006).  
 [15] E. C. Montenegro, *J. Phys.: Conf. Ser.* **194**, 012049 (2009).  
 [16] A. C. Tavares, H. Luna, W. Wolff, and E. C. Montenegro, *Phys. Rev. A* **92**, 032714 (2015).  
 [17] H. Luna, W. Wolff, E. C. Montenegro, A. C. Tavares, H. J. Ludde, G. Schenk, M. Horbatsch, and T. Kirchner, *Phys. Rev. A* **93**, 052705 (2016).  
 [18] J. Suárez, L. Méndez, and I. Rabadán, *J. Phys. Chem. Lett.* **6**, 72 (2015).  
 [19] I. Powis and D. J. Reynolds, *J. Chem. Soc., Faraday Trans.* **87**, 921 (1991).  
 [20] A. L. F. de Barros, J. Lecointre, H. Luna, M. B. Shah, and E. C. Montenegro, *Phys. Rev. A* **80**, 012716 (2009).  
 [21] F. Alvarado, R. Hoekstra, and T. Schlathölter, *J. Phys. B* **38**, 4085 (2005).  
 [22] S. Legendre, E. Giglio, M. Tarisien, A. Cassimi, B. Gervais, and L. Adoui, *J. Phys. B* **38**, L233 (2005).  
 [23] P. Sobocinski, Z. D. Pešić, R. Hellhammer, D. Klein, B. Sulik, J.-Y. Chesnel, and N. Stolterfoht, *J. Phys. B* **39**, 927 (2006).  
 [24] R. Cabrera-Trujillo, E. Deumens, Y. Öhrn, O. Quinet, J. R. Sabin, and N. Stolterfoht, *Phys. Rev. A* **75**, 052702 (2007).  
 [25] S. J. King and S. D. Price, *Int. J. Mass Spectrom.* **277**, 84 (2008).  
 [26] R. Singh, P. Bhatt, N. Yadav, and R. Shanker, *J. Phys. B* **46**, 085203 (2013).  
 [27] Natalia Ferreira, L. Sigaud, V. L. B. de Jesus, A. B. Rocha, L. H. Coutinho, and E. C. Montenegro, *Phys. Rev. A* **86**, 012702 (2012).  
 [28] Natalia Ferreira, L. Sigaud, and E. C. Montenegro, *J. Phys.: Conf. Ser.* **488**, 012042 (2014).  
 [29] L. Sigaud, Natalia Ferreira, L. H. Coutinho, V. L. B. de Jesus, and E. C. Montenegro, *J. Phys. B* **45**, 215203 (2012).  
 [30] L. Sigaud, V. L. B. de Jesus, Natalia Ferreira, and E. C. Montenegro, *Rev. Sci. Instrum.* **87**, 083112 (2016).  
 [31] I. Ben-Itzhak *et al.*, *J. Phys. B* **29**, L21 (1996).  
 [32] A. C. Cameron and F. A. G. Windmeijer, *J. Econometrics* **77**, 329 (1997).  
 [33] Natalia Ferreira, L. Sigaud, and E. C. Montenegro, *J. Phys. Chem. A* **121**, 3234 (2017).  
 [34] P. J. Richardson, J. H. D. Eland, P. G. Fournier, and D. L. Cooper, *J. Chem. Phys.* **84**, 3189 (1986).  
 [35] D. Winkoun, G. Dujardin, L. Hellner, and M. J. Besnard, *J. Phys. B* **21**, 1385 (1988).  
 [36] J. Laksman, E. P. Månsson, A. Sankari, D. Céolin, M. Gisselbrecht, and S. L. Sorensen, *Phys. Chem. Chem. Phys.* **15**, 19322 (2013).

- [37] S. Martin, L. Chen, R. Brédy, J. Bernard, and A. Cassimi, *J. Chem. Phys.* **142**, 094306 (2015).
- [38] D. Oubaziz, M. A. Quinto, and C. Champion, *Phys. Rev. A* **91**, 022703 (2015).
- [39] H. E. Stanton and J. E. Monahan, *J. Chem. Phys.* **41**, 3694 (1964).
- [40] P. J. Chantry and G. J. Schulzt, *Phys. Rev.* **156**, 134 (1967).
- [41] A. G. Sage, T. A. A. Oliver, R. N. Dixon, and M. Ashfold, *Mol. Phys.* **108**, 945 (2010).
- [42] J. E. Reutt, L. S. Wang, Y. T. Lee, and D. A. Shirley, *J. Chem. Phys.* **85**, 6928 (1986).
- [43] F. Fiquet-Fayard and P. M. Guyon, *Mol. Phys.* **11**, 17 (1966).
- [44] A. J. Lorquet and J. C. Lorquet, *Chem. Phys.* **4**, 353 (1974).